Decorative black coatings on titanium surfaces based on hard bi-layered carbon coatings synthesized by carbon implantation

P. Gupta, F. Fang, S. Rubanov, T. Loho, A. Koo, N. Swift, H. Fiedler, J. Leveneur, P.P. Murmu, A. Markwitz, J. Kennedy

PII: S0257-8972(18)31270-2
DOI: https://doi.org/10.1016/j.surfcoat.2018.11.060
Reference: SCT 24026

To appear in: *Surface & Coatings Technology*

Received date: 2 October 2018
Revised date: 12 November 2018
Accepted date: 20 November 2018

Please cite this article as: P. Gupta, F. Fang, S. Rubanov, T. Loho, A. Koo, N. Swift, H. Fiedler, J. Leveneur, P.P. Murmu, A. Markwitz, J. Kennedy , Decorative black coatings on titanium surfaces based on hard bi-layered carbon coatings synthesized by carbon implantation. Sct (2018), https://doi.org/10.1016/j.surfcoat.2018.11.060

Decorative black coatings on titanium surfaces based on hard bi-layered carbon coatings synthesized by carbon implantation

P. Gupta[1], F. Fang[1], S. Rubanov[2], T. Loho[3], A. Koo[4], N. Swift[4], H. Fiedler[1], J. Leveneur[1,5], P. P. Murmu[1], A. Markwitz[1,5], J. Kennedy[1,5]

[1]Department of Materials and Air, National Isotope Centre - GNS Science, PO Box 31312, Lower Hutt 5010, New Zealand
[2]Advanced Microscopy Facility, Bio21 Institute, University of Melbourne, Victoria, 3010, Australia
[3]Department of Chemical and Materials Engineering, The University of Auckland, Auckland 1010, New Zealand
[4]Measurements and Standard Laboratory, Callaghan Innovation, Lower Hutt 5046, New Zealand
[5]The MacDiarmid Institute for Advanced Materials and Nanotechnology, SCPS – Victoria University, PO Box 600, Wellington 6140, New Zealand

Abstract

New approaches to synthesize decorative black coatings on metallic surfaces are of significant research and commercial interest to manufacturing industries. In this work, decorative hard black coatings were deposited on a titanium surface by carbon ion implantation at ambient temperature. A 10 keV C^+ beam was implanted on a Ti substrate to a fluence of 1 - 1.25 × 10^{18} C cm^{-2}. Rutherford backscattering spectrometry and transmission electron microscopy results show that the implantation resulted in a bi-layered coating structure with a ~ 50 nm amorphous carbon layer at the surface followed by a ~ 50 nm amorphous titanium carbide intermixing layer deposited on top of a crystalline Ti surface. Raman spectroscopy confirms the formation of carbide intermixing layer and shows that the amorphous carbon layer has 15 – 20 % sp^3 content. Nanoindentation measurements show that the surface hardness of the implanted surface has increased by 72%, from 3.7 to 6.6 GPa, upon carbon implantation. Scratch tests further demonstrate a reduction in coefficient of friction in the implanted surface by 25%, signifying an improvement in wear-resistance of the coated materials. Colorimetry measurements reveal that carbon implantation reduces the luminosity of the Ti surface from 77 to 49 and chromaticity from 4.67 to 1.36, confirming incorporation of black color on Ti surface. The results demonstrate that C implantation onto a Ti surface at high fluence results

in a black coating with high surface hardness and wear-resistance that can be employed in decorative surface applications for manufacturing industries.

Key words: Decorative black coatings; amorphous carbon; titanium carbide; ion implantation; nanoindentation; color measurements.

1. Introduction

Decorative coatings are heavily used in a large array of applications in the manufacturing industries. Their primary purpose is to enhance the visual appeal of consumer products. In addition, they are also used to enhance the durability of the products by increasing their surface hardness, wear-resistance and corrosion resistance [1-5]. Titanium based compounds and amorphous carbon (a:C) coatings are some of the most widely-used materials in decorative coatings [4, 6-11]. They exhibit good mechanical and chemical compatibility with many substrates and can produce a range of colors depending on their chemical composition or thickness [12, 13]. For example, titanium nitride (TiN) for gold color, titanium carbide (TiC) for grey, titanium carbonitride (TiCN) for bronze and titanium oxycarbide (TiCO) / titanium aluminum carbonitride (TiAlCN) for black [12]. They also exhibit good tribological properties yielding a durable surface finish.

Black coatings are widely used in industries manufacturing watches, jewelry, electronic gadgets and automobiles. Our focus is on black decorative coatings for titanium surfaces e.g., black titanium watches and rings. Currently, TiC, TiCO, TiAlCO and TiAlCON from titanium compounds and amorphous carbon are the material of choice for dark / black decorative coatings [14]. Thermal evaporation, reactive / magnetron sputtering and chemical vapor deposition (CVD) are commonly used in their production [6, 8, 11, 14-16]. TiC exhibits high hardness and wear-resistance but display more of a dark grey color rather than a black color [8, 14]. Oxygen incorporation into TiC results in black color but leads to reduced hardness and wear-resistance [8, 14]. TiAlCO and TiAlCON have demonstrated remarkable mechanical properties but their color is highly dependent on their chemical composition [14]. Highly reproducible commercial coatings thus require precise control over the stoichiometry of 4 – 5 different elements of the coating resulting in added complexity. Amorphous carbon coatings on the other hand are easy to produce and are mechanically hard but they have to be sufficiently thick (> 1 μm) to exhibit a black color [14, 17]. This leads to accumulation of

stress resulting in poor adhesion to the substrate. Production by PVD or CVD does not create the interfacial bonding layer necessary for high adhesion. This leads to delamination and short lifetime of the coatings [18].

This work aims at developing a new pathway to impart black color on Ti surface by carbon implantation. The resultant coating must be hard and wear-resistant. We aim to overcome the adhesion issues present in thick amorphous carbon coatings by (a) limiting the carbon layer thickness to 100 – 200 nm and (b) creating a strong interfacial bonding layer (TiC) that promote extensive bonding between the carbon layers and the substrate thereby preventing delamination. Generally, thick amorphous carbon coatings are required to impart black color on a metallic surface [13]. But we will use the combination of amorphous carbon and TiC interface to produce a wear-resistance black surface with significantly reduced coating thickness. In addition, by limiting the composition of the coating to Ti from the substrate and C from the ion beam, the synthesis procedure is devoid of chemically complex procedures generally required for complex Ti compounds used in black coatings. The fabrication pathway can thus be more easily scaled up for large area reproducible surface coatings for industrial applications.

2. Material and methods

Pure Ti metallic surfaces were implanted with energetic carbon ions (10 keV) to: (a) form a hard and wear-resistant titanium carbide intermixing layer that promotes adhesion [19], and (b) form a further 50 - 100 nm amorphous carbon (a:C) layer on top.

The composition, structure, chemical bonding, mechanical properties and color of the coatings formed by ion implantation were studied by Rutherford backscattering, cross-sectional transmission electron microscopy (TEM), Raman scattering, nanoindentation and reflection measurements, respectively. The elemental depth profiles from RBS were evaluated

along with analytical TEM and vibrational modes measured from Raman spectroscopy to provide an in-depth analysis of the composition and structure of the coatings. Nanoindentation measurements helped in analyzing the changes in surface hardness, elasticity and wear-resistance of the Ti surface upon carbon implantation. The color coordinates measured from reflection measurements were used to quantify and compare the degree of black color obtained from C implantation with other reported studies.

2.1 Synthesis

The low energy ion implanter system at GNS Science employing a Penning gas ion source was used for growing black coating on Ti [5, 20, 21]. The pure Ti metal substrates, with 1 × 1 cm^2 area and 0.1 cm thickness, were polished to a roughness < 10 nm. The substrates were then loaded onto the target holder in the implanter sample chamber at a base pressure of ~7 × 10^{-8} hPa. Carbon monoxide was used as the precursor gas in the ion source. With a 2-kV anode voltage and 0.03 T magnetic field strength, a carbon rich plasma was established at a CO gas pressure of 2 × 10^{-6} hPa. A positive ion beam was extracted from the ion source onto the injector system at 8 kV terminal voltage. The ion beam was focused by an Einzel lens system onto the center of a 90-degree dipole magnet with 40 cm radius to mass separate the constituent species of the ion beam. By selecting a magnetic field strength of 0.12 T, only 10 keV C^+ ions were allowed into the ion implanter beam line. The C^+ beam was then subsequently focused by electrostatic quadrupole lenses and steerers onto the Ti substrate in the sample chamber with a target current density of 4 μA cm^{-2}. The beam was scanned uniformly across the Ti substrate to ensure homogenous coverage from the ion beam. The ion fluence was measured by a charge integrator connected to the target holder. A - 400 V electron suppression voltage was employed to prevent samples from getting charged up due to electron emission. Figure 1 shows the polished unimplanted Ti substrate and samples implanted with fluence ≥ 10^{18} C cm^{-2}. Samples implanted with less than 10^{18} C cm^{-2} did not show black color and hence were not investigated further.

2.2 Characterization

To reveal the composition of the coating and the extent of intermixing with the underlying substrate, the detailed elemental depth profiles of the surface region of the coatings were measured by Rutherford backscattering spectrometry (RBS). A 2 MeV $^4He^+$ beam collimated to a 1 mm diameter spot was used for RBS. A silicon surface barrier detector with a 1 mm aperture and 0.45 sr solid angle for detection, was placed at a backscattering angle of 165^o to detect the backscattered He ions. The measurements were carried out at a pressure of 2×10^{-6} hPa. The depth resolution of the measurements is primarily limited by the energy resolution of the detector which for our measurements are 20 keV [22]. The error margin for measuring elemental concentration in RBS is defined by statistical noise. For a signal strength of N counts, the error is given by $\frac{\sqrt{N} \times 100\%}{N}$. A reference target made of 400 nm Si_3N_4 layer on Si substrate was used to calibrate the spectra and eliminate the errors associated with the instrument. Each spectrum was collected for an accumulated charge of 40 μC.

For TEM measurements, after ion implantation the Ti samples were sputter coated with thin Au film followed by a carbon film to avoid charging effects during TEM sample preparation. Cross-sectional TEM samples were prepared using lift-out technique, described elsewhere [23]. The TEM samples were examined using FEI Tecnai F20 transmission electron microscope operated at 200 kV. Electron energy loss spectroscopy (EELS) measurements were conducted in STEM mode, with a 1 nm probe beam diameter, convergence semi-angle of 3.5 mrad and collection semi-angle of 16 mrad at 300 kV (Tecnai F30) using Gatan GIF Quantum™ 965 energy filter. All TEM and EELS analyses were carried out using Gatan Digital Micrograph software. Elemental profiles were extracted from electron energy loss spectrum image using energy windows 290-303 eV for carbon K-edge and 456-469 eV for Ti L-edge.

To ascertain the presence of TiC and investigate the quality of the deposited DLC films, the vibrational density of states of implanted and unimplanted Ti substrates were measured by Raman scattering using a confocal Raman microscope. Under 100× objective lens, 1 mW argon laser (514 nm – most studied for carbon materials [24]) was used to excite the sample. The scattered light was detected by a liquid nitrogen cooled CCD detector in a backscattering geometry. The signal from each sample was measured for 60 s and repeated 3 times for each Raman spectrum. Crystalline Si substrate was used as a reference to calibrate the Raman spectrometer. The resolution of the CCD detector is 1 cm^{-1}.

The mechanical properties of the samples were investigated with a Hysitron TI950 Triboindenter. Five sets of 9 indents at different loads were done at five random locations on each sample. Relatively featureless areas were chosen for all tests with optical microscopy and Scanning Probe Microscopy (SPM) in order to minimize the roughness effect on the nanoindentation and nanoscratch results [25]. All indents were done using a load-controlled feedback loop, with loads varying from 1 mN to 9 mN. Indentations were performed using a diamond Berkovich tip that has the same projected area-to-depth ratio as the Vickers indenter tip commonly used in microhardness testing. The results are shown as hardness and reduced modulus values obtained at different penetration depths.

The hardness and reduced modulus values for each indent were calculated using the Oliver-Pharr method from the unloading curve of the load-displacement curve [26], assuming a purely elastic unloading curve (reversible plastic deformation is negligible).

The coefficient of friction was measured by nanoscratch measurements using the same equipment. A diamond conical tip with a 1 μm radius of curvature was used. Five sets of 5 scratches at five random areas were performed on each sample. As with the nanoindentation tests, relatively featureless areas were chosen with optical microscopy and SPM in order to minimize roughness effects [25]. Each scratch was carried out with a constant normal load of

1 mN and a scratch distance of 10 µm. The normal force was capped at 1 mN to limit the penetration depth to the coating and minimize substrate effects [27].

For each scratch, a 2-dimensional 3-plate capacitive transducer measures the lateral force experienced by the probe during nanoscratch [27]. The nanoscratch load function consists of four segments: tilt measurement, loading, scratching, and unloading. The coefficient of friction (CoF) is calculated only from the scratching segment with the formula [28]:

$$CoF = \frac{Lateral\ Force\ (\mu N)}{Normal\ Force\ (\mu N)}$$

SPM images (20 × 20 µm^2) were obtained before and after indentation and scratch measurement, on each area of measurement. The SPM images were then used to determine whether a result is trustworthy or not. Results from tests where the diamond tip hit a surface asperity or contamination (if any) were not considered in this study.

The last investigation performed on the set of samples were colorimetry measurements. The color of coatings in the field of decoration are quantified in CIELAB 1976 color space which is based on human perception of color. This system of measurement uses three parameters. The first parameter, L^*, is a measure of lightness of an object. The other parameters, a^* and b^* represent color saturation of the sample in red-green and yellow-blue axis respectively. The chroma of the sample is given by chromaticity, C^*, which is,

$$C^* = \sqrt{(a^*)^2 + (b^*)^2}$$

An object is considered black for a human observer when C^* is close to 0 and L^* is less than 50 [16].

The L*, a* and b* values of the unimplanted and implanted Ti surfaces were measured using a MINOLTA CM-2500d portable spectrophotometer. This instrument measures spectral

reflectance, over the wavelength range 360 nm to 740 nm, under diffuse illumination and 8° viewing angle geometry (specular reflectance included and excluded).

3. Theory - Monte Carlo simulation of ion-solid interactions

The deposition process by carbon implantation was simulated using the Monte-Carlo based Dynamic Transport and Range of Ions in Matter (DTRIM) simulation code to understand the growth process [29]. The experimental parameters were provided as input to the code. The simulation was performed for an area of 10,000 $Å^2$ to get accurate results. The input parameters are shown in table I.

The key result of interest from the simulation is the elemental depth profile of C and Ti in the surface region. Figure 2 shows the depth profile in the top 150 nm of implanted Ti surface. Depth in nm was calculated from depth in areal atomic density ($\times 10^{15}$ atoms cm^{-2}) by the relation [30],

$$Depth\ (nm) = \frac{Depth\ (10^{15}\ atoms\ cm^{-2})}{Atomic\ density\ (10^{22}\ atoms\ cm^{-3})}$$

Note however, that DTRIM operates on an assumed density value (4.5 g cm^{-3}) provided as input for the simulation.

The projected range and straggling of 10 keV carbon atoms in titanium are 22 nm and 17 nm respectively. At low fluence, the concentration profile of C in Ti will have a Gaussian shape with the peak concentration at depth of 22 nm inside Ti substrate. As the fluence increases, the width of the Gaussian profile extends and reaches the surface [31]. The sputter yield of C on C is 0.4 and C on Ti is 0.6. Hence the surface gets quickly depleted out of Ti and leads to formation of a carbon rich surface. Since the sputter yield of the process is < 1, the implantation leads to growth of carbon layers leading to formation of coating [20, 31].

Unlike other deposition processes, C atoms penetrate much deeper into the Ti substrate leading to an intermixing titanium carbide layer upon which the carbon layers grow. For 1×10^{18} C cm^{-2}, the simulation predicts a 60-nm thick carbon rich layers and 40 – 60 nm thick TiC intermixing layer. As the fluence increases to 1.25×10^{18} C cm^{-2}, the major change observed is the increase in the thickness of carbon layer by 20 nm (150×10^{15} atoms cm^{-2}) indicating a sputter yield of 0.4. Thus, implanting further will lead to thicker a:C films but the carbide intermixing layer will remain largely unaffected. For such a thin deposition, the a:C films are expected to contain low levels of Ti (~7 at.%) in the surface region.

4. Results and Discussion

4.1 Rutherford backscattering spectrometry

RBS provides the actual depth profile of Ti and C in the implanted surface which can then be compared with the simulation results. Figure 3 shows the RBS spectra of the unimplanted and C implanted Ti substrates. The spectrum records the energy and intensity of He ions backscattered from the samples in the abscissa and ordinate respectively.

In the RBS spectrum of unimplanted Ti, the signals were observed to rise from 1.44 MeV which denotes He ions backscattered from the Ti surface. The energy of signal onset is characteristic for Ti, as the kinematic factor (K) for He^+ ion backscattering from Ti atoms at an angle of 165^o is 0.72 [32]. The intensity of the signal corresponds to the concentration of Ti in the sample, which is 100 at.% in this case. As He ions penetrate deeper into the sample they lose energy, primarily by electronic stopping, and the backscattered ions are therefore detected at lower energies. The reduction in energy due to electronic stopping results in increased cross-section for ion-solid interaction and thus accounts for the increase in signal strength with depth of the sample. The RBS spectra are fit with simulated target profiles using Rutherford Universal Manipulation Program (RUMP) to determine the chemical composition

and depth profiles of the examined samples [33]. RBS spectrum of unimplanted Ti substrate was satisfactorily fit with a simulated target made of a 2 μm thick (analysis depth of 2 MeV He^+ beam; simulation not shown) pure Ti.

RBS spectra of 1×10^{18} and 1.25×10^{18} C cm^{-2} implanted samples are plotted on top of unimplanted Ti spectrum in figure 3. The onset of signals in 1×10^{18} and 1.25×10^{18} C cm^{-2} implanted samples are measured to be shifted from Ti surface energy (1.44 MeV) by 0.04 and 0.05 MeV, respectively. This shows that the implanted sample surface is not composed of Ti and confirms the deposition of a coating layer. The coating layer thickness is proportional to the magnitude of shift observed in Ti signal from the Ti surface energy.

The coating composition can be inferred from the sharp rise in signal intensity observed at 0.51 MeV for both the implanted samples. The signal energy corresponds to backscattering energy of He^+ ions from carbon atoms at the surface (K = 0.255 [32]) which is expected in our study. Since carbon is a light element, its cross-section of collision with He^+ ions are significantly smaller than Ti which leads to low intense signals as observed from figure 3.

The extent of intermixing between carbon and titanium can be deduced from the slope of the Ti edge shown in the inset. In absence of any intermixing, the spectra must be satisfactorily fit with a simulated target composed of two layers: layer 1 – C and layer 2 – Ti. However, it can be clearly observed in the inset that the Ti edge has greater slope, and for a satisfactory fit, the simulation must account for an interface layer made partly of Ti and C. This agrees with DTRIM simulations which predicts a Ti-C intermixed interface layer. The details of the fits used for the implanted samples are shown in table II.

A five layered RUMP fit describes the RBS data within the error margins (ΔE: 20 keV, ΔC = 10 at.%, ΔTi = 2.5 at.%). A pure carbon layer is observed at the surface in both the implanted samples. As the carbon implantation fluence increases by 2.5×10^{17} C cm^{-2}, the thickness of the pure carbon layer increases by 1.5×10^{17} atoms cm^{-2}. The sputtering yield of carbon on

carbon can thus be estimated to be ~ 0.4 which corresponds well with DTRIM calculation. However, DTRIM predicts a Ti surface concentration to be 8 – 10 at.% which is not observed in RBS measurement (indicating a surface Ti concentration < 2.5 at.%). This shows that C on Ti sputter yield is higher than that predicted in DTRIM.

The chemical composition and areal density of the underlying carbide layers were found to be same for both the implanted samples as computed by DTRIM. The extent of intermixing between Ti and C can be extrapolated from the RBS spectra. The intermixing layer is composed of 40 at.% C and 60 at.% Ti and areal density of the intermixing layer was measured to be 2.7×10^{17} atoms cm^{-2}. The measured results agree with DTRIM simulation results within the experimental errors. This intermixing is advantageous for two reasons: First, it is expected to promote strong adhesion between Ti and the a:C layer. Achieving strong adhesion between a:C and a metallic substrate is usually difficult in PECVD or PVD processes. Secondly, the intermixing will promote formation of TiC which is reported to be extremely hard and show grey color [8, 14].

4.2 Transmission Electron Microscopy

RBS measurements do not yield information on physical characteristics such as thickness (in nm), density and microstructure of the deposited coatings. Hence, cross-sectional TEM and STEM measurements were used to perform localized analysis on the microstructure of the bi-layered structure formed on Ti surface.

Figure 4 shows the cross-section of Ti surface implanted with carbon to a fluence of 1×10^{18} C cm^{-2}. The inset shows the elemental profile obtained from electron energy loss spectrum image (not shown) and is overlaid on top of the cross-sectional image to show the variation in chemical composition of the implanted sample. The top most layers Pt/C/Au were deposited during TEM sample preparation for lift-off. The carbon layers beneath the Au layer is the a:C layer formed by C implantation. The a:C region begins from the surface and extends ~ 50 - 60

nm towards the Ti substrate. At depths greater than that, significant Ti concentration (> 10 at.%) in the a:C layers can be observed (as dark precipitates in TEM image and is confirmed in the elemental profile). This region denotes the onset of TiC region as measured from RBS and extends ~ 30 - 40 nm further down towards the Ti substrate. The carbon concentration drops from 90 at.% to less than 5 at.% with depth in the TiC region.

The TEM results agree well with the RBS interpretation and confirms the presence of bi-layered (C/TiC/Ti) structure on the surface of implanted Ti samples. Comparison of TEM results with RBS allow us to identify the density of the a:C and TiC layers making up the surface which is useful for identifying the physical characteristics of the coatings. By comparing and correlating the layer thicknesses of a:C and the intermixing TiC layer, we obtain the density of the a:C layer to be 2.6 ± 0.3 g cm^{-3} and TiC layer to be 4.3 ± 0.7 g cm^{-3}. The density of a:C layers correspond to a carbon layer with high hardness. The deduced results from TEM and RBS comparison can be ascertained by Raman spectroscopy.

4.3 Raman Spectroscopy

Figure 5 shows the Raman spectra for unimplanted and implanted Ti samples. The peaks recorded in the spectra correspond to active Raman vibrational modes of the sample. Unimplanted Ti does not show any peaks within the investigated region which is in agreement with literature [34]. The implanted samples however exhibit a range of peaks within 200 – 1800 cm^{-1}. The observed Raman modes can be classified into two regions: (a) peaks lying in 200 – 900 cm^{-1} regions arising from carbide phases; (b) peaks lying in 1000 – 1800 cm^{-1} arising from amorphous carbon.

Stochiometric TiC does not have Raman active vibrational modes. Raman modes are observed in TiC only in the presence of disorder induced by carbon vacancies. Carbon vacancies leads to inversion symmetry breaking resulting in E_g, A_{1g} and T_{2g} vibrational modes [35, 36]. As observed from RBS measurements, the interfacial layer has a composition of

$TiC_{0.67}$. Raman spectra of $TiC_{0.67}$ was reported to show peaks centered at 265, 340, 372, 596, and 661 cm^{-1} [36]. However, presence of large clusters of carbon vacancies leads to peak broadening and overlapping [35, 36]. The extent of overlap depends on the density of carbon vacancies and amorphous nature of the sample. In this case, the amorphization and vacancy density is high enough causing complete overlap of peaks centered around 265, 340 and 372 cm^{-1} leading to a broad peak from 200 – 500 cm^{-1} and overlap of peaks centered around 596 and 661 cm^{-1} leading to a second broad peak from 500 – 900 cm^{-1}. A key conclusion thus derived from Raman investigation is that carbon ion implantation into Ti substrate leads to formation of an intermixing layer made of TiC. This result confirms the interpretation of a bi-layered coating structure derived from DTRIM, RBS and TEM investigations. Furthermore, both the implanted samples show similar peaks in accordance to our previous observation that the interfacial carbide layers formed in both the samples are of the same composition, and phase.

The peaks observed from 1000 – 1800 cm^{-1} arises from the vibration modes of amorphous carbon layer. Under laser excitation from visible region, amorphous carbon exhibits two Raman active vibrational modes: E_{2g} mode (G peak - centered ~ 1500 - 1650 cm^{-1}) arising from the stretching of sp^2 bonded carbon atoms and A_{1g} mode (D peak - centered ~ 1350 cm^{-1}) arising from the breathing modes of aromatic carbon rings [24, 37]. Vibrational modes of sp^3 bonded carbon can only be observed under UV laser excitation as the band gap of sp^3 bonded carbon lies in the deep UV region [37]. The G peak position in the spectrum and the ratio of intensity of G peak to D peak (I(D)/I(G)) can help us estimate the sp^2:sp^3 ratio and sp^2 cluster size of the carbon layers [24, 37]. These properties play a dominant role in determining the physical, electrical and optical properties of the carbon layers.

The Raman spectra arising from amorphous carbon layers are shown in figure 6 and are fit with a Breit-Wigner-Fano (BWF) line shape for G peak and Lorentzian line shape for D peak [24, 37]. A BWF and Lorentzian fit describe the Raman spectra of amorphous carbon much

better than a simple multi-peak Gaussian or Lorentzian fit. The Gaussian fit tends to overestimate the contribution from D peak and the BWF fit allows accounting for the asymmetrical nature of the G peak [24, 38, 39]. The key parameters required from the fits are G peak position and I(D)/I(G) ratio shown in table III.

The variation in Raman parameters can be correlated with changes in the sp^2 cluster size, orientation, bond disorder and sp^2/sp^3 ratio of the amorphous carbon films by making use of the three-stage model proposed by Robertson and Ferrari [24]. They define an amorphization trajectory for carbon as it transforms from,

1) Graphite → nanocrystalline graphite
2) Nanocrystalline graphite → amorphous carbon
3) Amorphous carbon → tetrahedrally coordinated amorphous carbon.

The three-stage model correlates the change in G peak position and I(D)/I(G) ratio of carbon films with the sp^2 cluster size and sp^2:sp^3 ratio along the amorphization trajectory of carbon through the three stages. By comparing with the three-stage model, the amorphous carbon layers of both the samples falls under the stage 2 process with sp^3 fraction in between 15 – 20 %. As the implantation fluence increases, the total number of carbon atoms increases leading to a rise in the G peak intensity. The D peak intensity on the other hand, decreases. This indicates a reduction in sp^2 cluster size and quantity. The D peak is broad in both cases indicating presence of sp^2 clusters with a range of sizes. The I(D)/I(G) ratio can be correlated to the cluster size using the following relation [24],

$$\frac{I(D)}{I(G)} = C'(\lambda) L_a^2$$

Where $C'(\lambda)$ for 514 nm laser is 0.0055 and L_a is the sp^2 cluster size or diameter. Using the above equation, the average sp^2 cluster sizes are calculated to be 13 ± 0.3 Å for 1×10^{18} C cm^{-2} sample and 11 ± 0.5 Å for 1.25×10^{18} C cm^{-2}. Thus, growth of carbon layers with ion

implantation shows an overall increase in sp^3 nature of the films. In addition, in our RBS-TEM investigation we established the density of the films to be 2.6 ± 0.3 g cm^{-3}, which also suggests the carbon atoms to be densely packed within the layers. Amorphous carbon with these properties usually display high hardness values and low coefficient of friction.

4.4 Nanoindentation

To validate that such tribological properties were produced with this ion implantation method, the hardness and elastic modulus of the samples were measured using nanoindentation. The hardness and reduced modulus results are shown in figure 7.

Carbon implanted Ti show a hardness of 6 – 7 GPa at the surface and decrease as the maximum indentation depth increases. Hardness of unimplanted Ti was measured to be 3.7 ± 0.2 GPa and does not change with depth. This indicates that the value measured is representative of the bulk hardness of Ti. When the hardness of the coated sample decreases to this number (3.7 ± 0.2 GPa), it can be assumed that this value is due to the bulk Ti substrate and not from the surface.

The results show that the surface of C implanted Ti are harder than unimplanted Ti surface. Carbon implantation on Ti surface has increased the surface hardness of the material by approximately 72%. This increase in hardness is observed to a maximum indentation depth of approximately 200 nm. At deeper depths (> 150 – 200 nm), the indenter reached the substrate and there are no significant differences between the implanted and unimplanted sample. This suggests that the thickness of the modified surface is approximately 150-200 nm as confirmed by TEM.

There are no significant differences in the reduced modulus values for all three samples at all measured depth. This suggests that the C ion implantation process did not modify the bond strength of the Ti-Ti bond in the metal lattice by any significant amount.

The reduced modulus values for all samples increases as the indentation depth increases. This can be attributed to the polishing procedure performed on the Ti surface. Mechanical polishing is known to introduce some residual tensile stresses that can alter the surface mechanical properties of the sample. This suggests that the higher reduced modulus values at deeper depths are from the residual stress-free regions of the bulk Ti substrate [27, 40].

Figure 8 shows that the C implanted Ti possess significantly lower CoF (0.15 ± 0.02 for 1×10^{18} C cm^{-2} and 0.14 ± 0.01 for 1.25×10^{18} C cm^{-2}) than unimplanted Ti (0.21 ± 0.03). The results imply that for the same applied normal force, C implanted samples exhibit a smaller lateral force, and hence lesser wear, than unimplanted Ti surface. While the diamond-Ti contact is unlikely to be the type of interactions used in practical applications, this result provides a useful measurement of the improvements in surface wear-resistance properties upon C implantation.

4.5 Color measurement

The final study performed on the samples in this work were the CIELAB 1976 color measurements. They were used to quantify the color of implanted Ti surface. Table IV shows the value obtained from the three samples (unimplanted Ti, 1×10^{18} and 1.25×10^{18} C cm^{-2} implanted samples).

The reflectance measurements represent the color of the samples in the CIELAB 1976 color space by primarily using luminosity (L^*) and chromaticity ($C^* = \sqrt{a^* + b^*}$). The luminosity indicates the brightness of the surface and chromaticity denotes the color saturation of the sample. A material is classified as black if the luminosity of the material is less than 0.5 and chromaticity is close to 0. The data can be interpreted by including or excluding specular reflectance. Since the signal intensity is very weak in the latter case, we have focused on the measurements that includes specular reflectance.

In this mode, two different standard observers were used: 2^o and 10^o observers (2^o results not shown). In both these geometries, the luminosity of the Ti surface reduced from ~ 77 to 49 for 1×10^{18} C cm^{-2} and to 50 for 1.25×10^{18} C cm^{-2}. The chromaticity of the Ti surface also decreased from 4.6 to 1.4 for 1×10^{18} C cm^{-2} and to 2.3 for 1.25×10^{18} C cm^{-2}. The results show that the carbon implantation yields a black surface for 1×10^{18} C cm^{-2} and a dark-grey surface for 1.25×10^{18} C cm^{-2}.

The black color of the surface arises from the low reflectance and the high absorption of light by the thin coating layers. Presence of a high fraction of sp^2 hybridized carbon in the a-C layer results in a low optical bandgap [41]. This leads to increased light absorption. Generally, sp^2 rich carbon films are avoided as they do not cause significant rise in surface hardness. However, presence of a hard TiC interface layer in the coating structure allows use of sp^2 rich a-C layers without compromising on the mechanical properties of the coated substrate. In addition, TiC has much lower reflectance than Ti metal which further contributes to the black color of the surface [42, 43]. Thus, the bi-layer structure composed of a-C surface layer and TiC interface layer has higher absorbance, lower reflectance and better wear-resistance than an independent a-C coating or TiC coating with similar thickness.

Table IV also compares the measured L^* and C^* values with that reported in literature for TiCO and TiCON films. The colorimetry values measured for 1×10^{18} C cm^{-2} is comparable to other reported values. Oxygen incorporation is reported to cause a greater decrease in the luminosity of the Ti surface. However, the chromaticity of C implanted films is lower compared to literature values (excluding Ono et al. [8]).

It must be emphasized that the samples prepared in this work do not contain oxygen. As stated in the review of black coatings [14], incorporation of oxygen may result in blacker Ti surfaces but they cause reduction in the hardness and wear-resistance of the coatings. We show that by mere carbon implantation we can produce a black surface comparable to that of

TiCO in literature, while simultaneously enhancing the mechanical hardness and wear-resistance of the Ti surface.

5. Conclusion

In this work, we have demonstrated an ion beam approach to combine the two current approaches (a:C coating and Ti compound coating) to impart black color to Ti surfaces. By implanting pure Ti with carbon ions at 10 kV acceleration and to a fluence $\geq 1 \times 10^{18}$ C cm^{-2}, a black wear-resistant coating was established. The coating was composed of a:C/TiC/Ti bi-layered structure. The density of the a:C layer was measured to be 2.6 ± 0.3 g cm^{-3} and the intermixing carbide layer was measured to have a density of 4.3 ± 0.7 g cm^{-3}. Raman spectroscopy confirms the presence of bi-layered structure and indicates that the a:C layer is composed at least of 15 – 20% sp^3 carbon. The surface hardness of Ti surface improved by 72% and coefficient of friction decreased by 25 – 30 % upon carbon implantation. The implantation also reduced the brightness and chromaticity of titanium leading to a black surface. Future work will focus on establishing an industry prototype that can replicate the synthesis protocol demonstrated in this work on large metallic surfaces with a simplified experimental setup. In addition, as Ti alloys are often used instead of pure Ti, we will investigate the effect of C implantation on their structural, mechanical and optical properties.

6. Acknowledgements

We would like to acknowledge the technical support from Chris Purcell from GNS Science. This work is part of the TiTeNZ program (UOWX1402) funded by the Ministry of Business, Innovation and Employment, New Zealand.

References

[1] E. Budke, J. Krempel-Hesse, H. Maidhof, H. Schüssler, Surface and Coatings Technology, 112 (1999) 108-113.

[2] N.H. Chen, C.J. Chung, C.C. Chiang, K.C. Chen, J.L. He, Surface and Coatings Technology, 236 (2013) 29-35.

[3] P.J. Kelly, R.D. Arnell, Vacuum, 56 (2000) 159-172.

[4] J. Vetter, Surface and Coatings Technology, 257 (2014) 213-240.

[5] A. Markwitz, J. Kennedy, Nuclear Instruments and Methods in Physics Research Section B: Beam Interactions with Materials and Atoms, 409 (2017) 86-90.

[6] R. Constantin, P.A. Steinmann, C. Manasterski, Decorative PVD Coatings, in: Nanomaterials and Surface Engineering, 2013, pp. 109-161.

[7] L. Milschi, I. Belahsen, G.C. Lain, S.S. Tomiello, C.D. Boeira, L.T. Bim, F. Cemin, C.M. Menezes, B.L. Perotti, J. Catafesta, C.A. Figueroa, Surface Engineering, 34 (2018) 562-568.

[8] K. Ono, M. Wakabayashi, Y. Tsukakoshi, Y. Abe, Applied Surface Science, 364 (2016) 69-74.

[9] M. Panjan, M. Klanjšek Gunde, P. Panjan, M. Čekada, Surface and Coatings Technology, 254 (2014) 65-72.

[10] L. Skowronski, A.A. Wachowiak, K. Zdunek, M. Trzcinski, M.K. Naparty, Thin Solid Films, 627 (2017) 1-8.

[11] C. Mitterer, PVD and CVD Hard Coatings, in: Comprehensive Hard Materials, 2014, pp. 449-467.

[12] U. Beck, G. Reiners, I. Urban, K. Witt, Thin Solid Films, 220 (1992) 234-240.

[13] M. Clapa, S. Mitura, P. Niedzielski, A. Karczemska, J. Hassard, Diamond and Related Materials, 10 (2001) 1121-1124.

[14] J. Takadoum, The European Physical Journal-Applied Physics, 52 (2010).

[15] J.M. Chappé, M.C. Marco de Lucas, L. Cunha, C. Moura, J.F. Pierson, L. Imhoff, O. Heintz, V. Potin, S. Bourgeois, F. Vaz, Thin Solid Films, 520 (2011) 144-151.

[16] J.M. Chappé, F. Vaz, L. Cunha, C. Moura, M.C. Marco de Lucas, L. Imhoff, S. Bourgeois, J.F. Pierson, Surface and Coatings Technology, 203 (2008) 804-807.

[17] B. Singh, S. McClelland, F. Tams, B. Halon, O. Mesker, D. Furst, Applied Physics Letters, 57 (1990) 2288-2290.

[18] E. Ali, D. Christophe, Journal of Physics D: Applied Physics, 39 (2006) R311.

[19] D.E. Wolfe, J. Singh, Surface and Coatings Technology, 124 (2000) 142-153.

[20] A. Markwitz, B. Mohr, J. Leveneur, Nuclear Instruments and Methods in Physics Research, Section B: Beam Interactions with Materials and Atoms, 331 (2014) 144-148.

[21] A. Markwitz, J. Kennedy, International Journal of Nanotechnology, 6 (2009) 369-383.

[22] J. Kennedy, A. Markwitz, H.J. Trodahl, B.J. Ruck, S.M. Durbin, W. Gao, Journal of Electronic Materials, 36 (2007) 472-482.

[23] L.A. Giannuzzi, J.L. Drown, S.R. Brown, R.B. Irwin, F.A. Stevie, Microscopy Research and Technique, 41 (1998) 285-290.

[24] A.C. Ferrari, J. Robertson, Physical review B, 61 (2000) 14095.

[25] L. Chen, A. Ahadi, J. Zhou, J.-E. Ståhl, Procedia CIRP, 8 (2013) 334-339.

[26] W.C. Oliver, G.M. Pharr, Journal of Materials Research, 19 (2004) 3-20.

[27] A.C. Fischer-Cripps, Nanoindentation Instrumentation, in: Nanoindentation, Springer, 2011, pp. 199-211.

[28] I. Hutchings, P. Shipway, 3 - Friction, in: I. Hutchings, P. Shipway (Eds.) Tribology (Second Edition), Butterworth-Heinemann, 2017, pp. 37-77.

[29] W. Möller, W. Eckstein, Nuclear Instruments and Methods in Physics Research Section B: Beam Interactions with Materials and Atoms, 2 (1984) 814-818.

[30] M. Nastasi, J. Mayer, J.K. Hirvonen, Ion-Solid Interactions: Fundamentals and Applications, Cambridge University Press, Cambridge, 1996.

[31] P.G. Sridhar Gupta, in: School of Chemical and Physical Sciences, Victoria University of Wellington, Wellington, New Zealand, 2017, pp. 255.

[32] Y. Wang, M.A. Nastasi, Handbook of modern ion beam materials analysis, Materials Research Society Warrendale, Pennsylvania, 2009.

[33] M. Thompson, L. Doolittle, Computer Graphic Service, Version 0.950, (2002).

[34] B. Lohse, A. Calka, D. Wexler, Journal of applied physics, 97 (2005) 114912.

[35] M. Klein, J.A. Holy, W. Williams, Physical Review B, 17 (1978) 1546.

[36] M. Amer, M.W. Barsoum, T. El-Raghy, I. Weiss, S. Leclair, D. Liptak, Journal of applied physics, 84 (1998) 5817-5819.

[37] A.C. Ferrari, Diamond and related materials, 11 (2002) 1053-1061.

[38] S. Prawer, K.W. Nugent, Y. Lifshitz, G.D. Lempert, E. Grossman, J. Kulik, I. Avigal, R. Kalish, Diamond and Related Materials, 5 (1996) 433-438.

[39] A. Eriksen Tell, in: Disciplinary Domain of Science and Technology, Technology, Department of Engineering Sciences, Solid State Electronics, Uppsala University, Uppsala, Sweden, 2017, pp. 43.

[40] H. Huang, H. Zhao, Z. Zhang, Z. Yang, Z. Ma, Materials, 5 (2012) 1033-1039.

[41] M. Chhowalla, J. Robertson, C. Chen, S. Silva, C. Davis, G. Amaratunga, W. Milne, Journal of applied physics, 81 (1997) 139-145.

[42] J. Pflüger, J. Fink, Determination of optical constants by high-energy, electron-energy-loss spectroscopy (EELS), in: Handbook of Optical Constants of Solids, Elsevier, 1997, pp. 293-311.

[43] P. Johnson, R. Christy, Physical Review B, 9 (1974) 5056.

[44] A.C. Fernandes, F. Vaz, L. Cunha, N.M.G. Parreira, A. Cavaleiro, P. Goudeau, E. Le Bourhis, J.P. Rivière, D. Munteanu, B. Borcea, R. Cozma, Thin Solid Films, 515 (2007) 5424-5429.

List of tables

Table I: Input parameters for the simulation of the growth of a:C / carbide layers on titanium substrate

Parameters	**Values**
Input Energy	10 keV
Ion	Carbon
Target	Titanium
Fluence	1 - 1.25 × 10^{18} C cm^{-2}
Density	4.5 g cm^{-3}
Simulation area	10000 $Å^2$

Table II: RUMP simulation – Target description for 1×10^{18} and 1.25×10^{18} C cm^{-2} implanted samples.

Layer	**Elemental composition**		**1×10^{18} C cm^{-2}**	**1.25×10^{18} C cm^{-2}**
	C (at.%)	**Ti** (at.%)	**Layer Thickness (**1×10^{15} atoms cm^{-2})	
1	100%	0%	100	250
2	95%	5%	200	200
3	90%	10%	300	300
4	40%	60%	270	270
5	0%	100%	10000	10000

Table III: Raman parameters obtained from fitting the D and G peaks of the a:C layers.

Parameters	**C = 1 × 10^{18} cm^{-2}**	**C = 1.25 × 10^{18} cm^{-2}**
G peak position	1553 ± 2 cm^{-1}	1538 ± 3 cm^{-1}
I(D)/I(G)	0.92 ± 0.02	0.64 ± 0.05
FWHM of G peak	186 ± 3 cm^{-1}	236 ± 4 cm^{-1}
sp^2 cluster size	13 ± 0.3 Å	11 ± 0.5 Å

Table IV: Color measurements (specular reflection included) from the spectrophotometer in CIELAB 1976 color space shows C implantation reduces the brightness (L*) and chromaticity of Ti surface.

Sample	**L^***	**a^***	**b^***	**C^***
	D65, 10^o observer			
Unimplanted Ti	77.20	1.24	4.50	4.67
1×10^{18} C cm^{-2}	48.98	-0.33	-1.32	1.36
1.25×10^{18} C cm^{-2}	49.99	0.30	2.24	2.26
Chappe et al., [16]	~42	-	-	1.87
Chappe et al., [15]	~48	-	-	~1.4
Fernandes et al., [44]	45.8	-	-	~1.7
Ono et al., [8]	41.5	-	-	0.62

Figure captions:

Figure 1: Pictures of polished Ti samples: (a) Unimplanted Ti substrate; (b) 1×10^{18} C cm^{-2} implanted Ti and (c) 1.25×10^{18} C cm^{-2} implanted Ti.

Figure 2: Calculated depth profiles of C and Ti for Ti surface implanted with 1 and 1.25×10^{18} C cm^{-2}. The depth axis in nm is calculated with a density of 4.5 g cm^{-3} for Ti, 4.3 g cm^{-3} for TiC and 2.6 g cm^{-3} for a:C.

Figure 3: RBS spectra of unimplanted and C implanted Ti substrates. The implanted Ti spectra were fit with simulated multi-layer fits of Ti/Ti-C/C structure (simulation 1 and 2). Inset: Ti edge from 1×10^{18} C cm^{-2} implanted sample is shown and compared with two different simulations: (1) DLC/TiC/Ti multi-layered fit; (2) DLC/Ti layered fit, to show the presence of intermixing carbide layer.

Figure 4: Cross-sectional TEM image of 1×10^{18} C cm^{-2} implanted Ti sample. The TEM cross section shows a bi-layered structure with crystalline Ti substrate at the bottom followed by amorphized region of TiC layers with varying stoichiometry ending with a:C region at the surface. The inset shows the elemental profiling of the same region using EELS in STEM mode.

Figure 5: Raman spectra of Ti surfaces implanted with carbon to a fluence of 1 and 1.25×10^{18} C cm^{-2}. Raman vibrational modes from carbide phase and carbon layers can be seen in the region 200 – 900 cm^{-1} and 1000 – 1800 cm^{-1}, respectively.

Figure 6: Raman spectra of amorphous carbon layers on Ti surface are fit with Breit-Wigner-Fano line shape and Lorentzian line shape to obtain the G and D peak parameters respectively. Figure 6 (a) and (b) shows the fits of Ti implanted with 1 and 1.25×10^{18} C cm^{-2} respectively.

Figure 7: (a) Hardness and (b) Reduced modulus as a function of depth for unimplanted and C implanted Ti surfaces.

Figure 8: Comparison of coefficient of friction at unimplanted and C implanted Ti surface.

List of figures

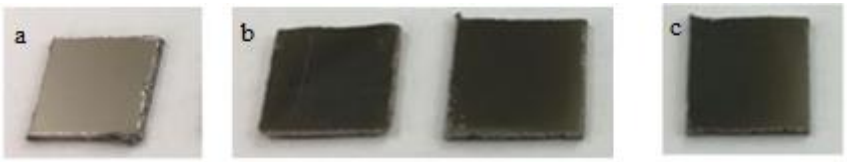

Figure 1 (color – online only)

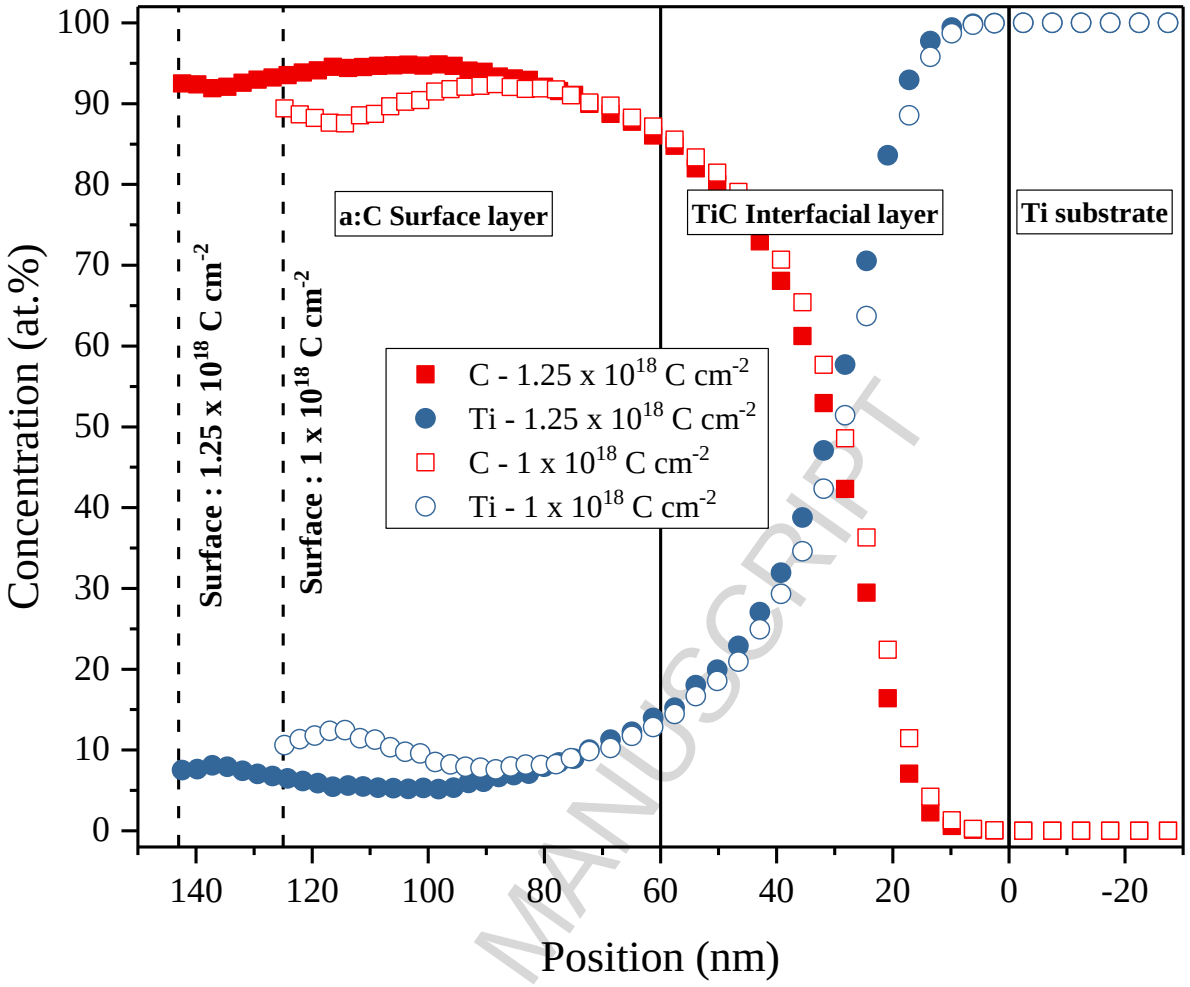

Figure 2 (color – online only)

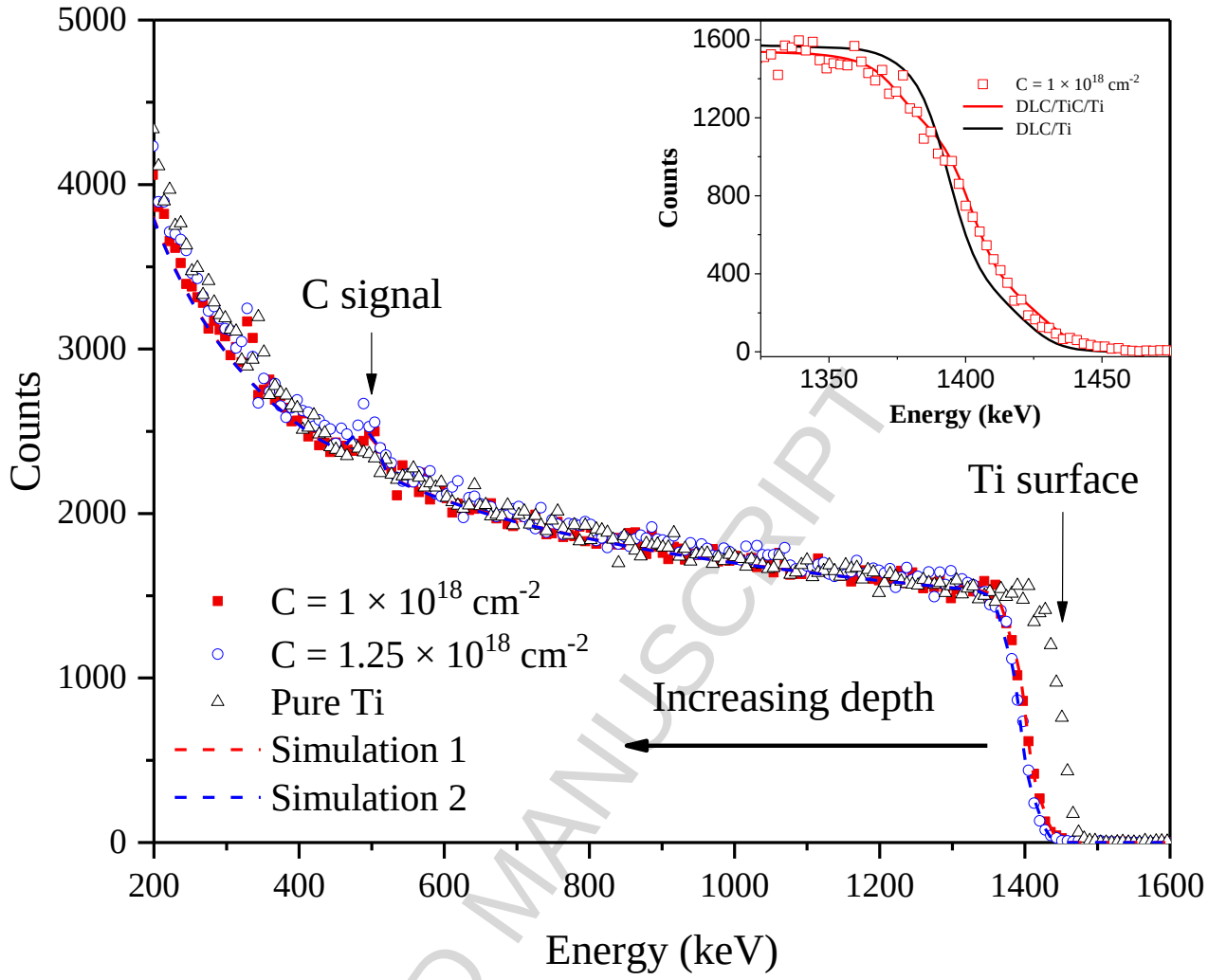

Figure 3 (color – online only)

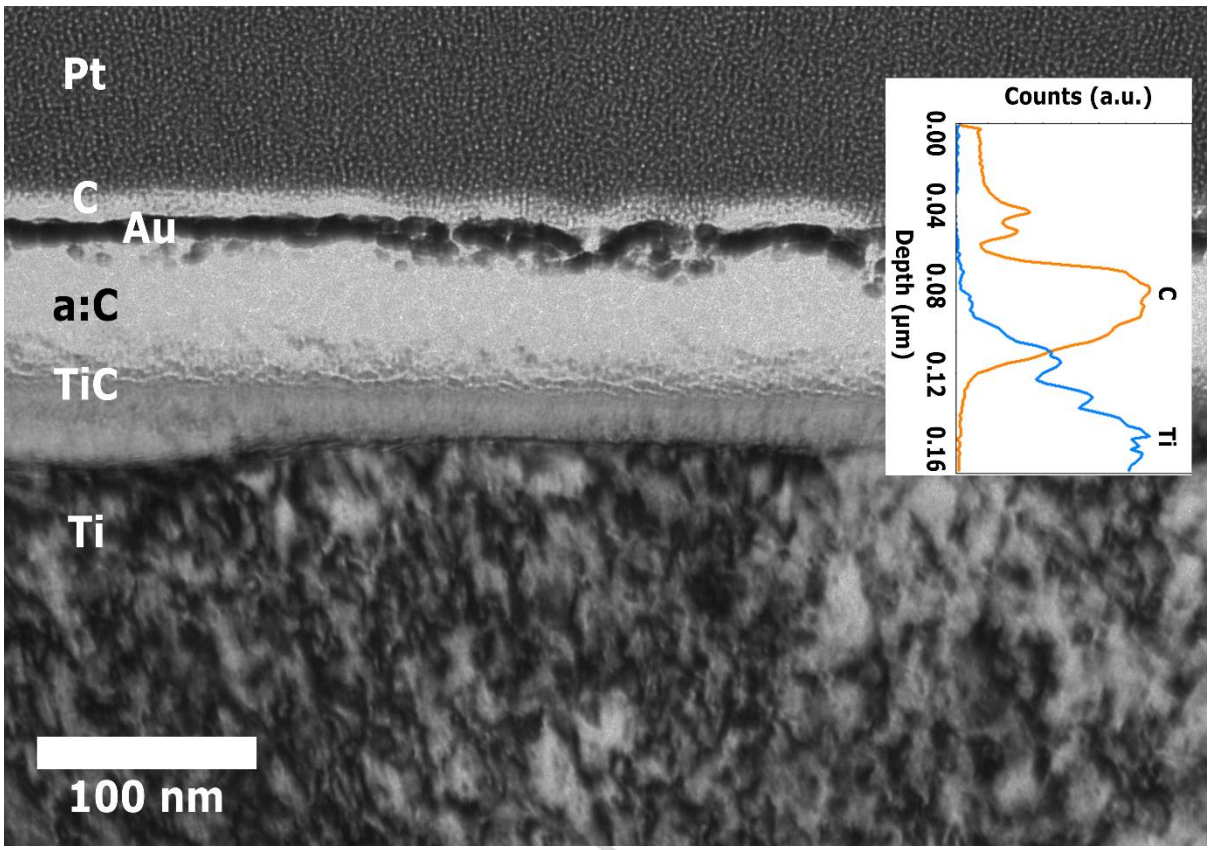

Figure 4 (color – online only)

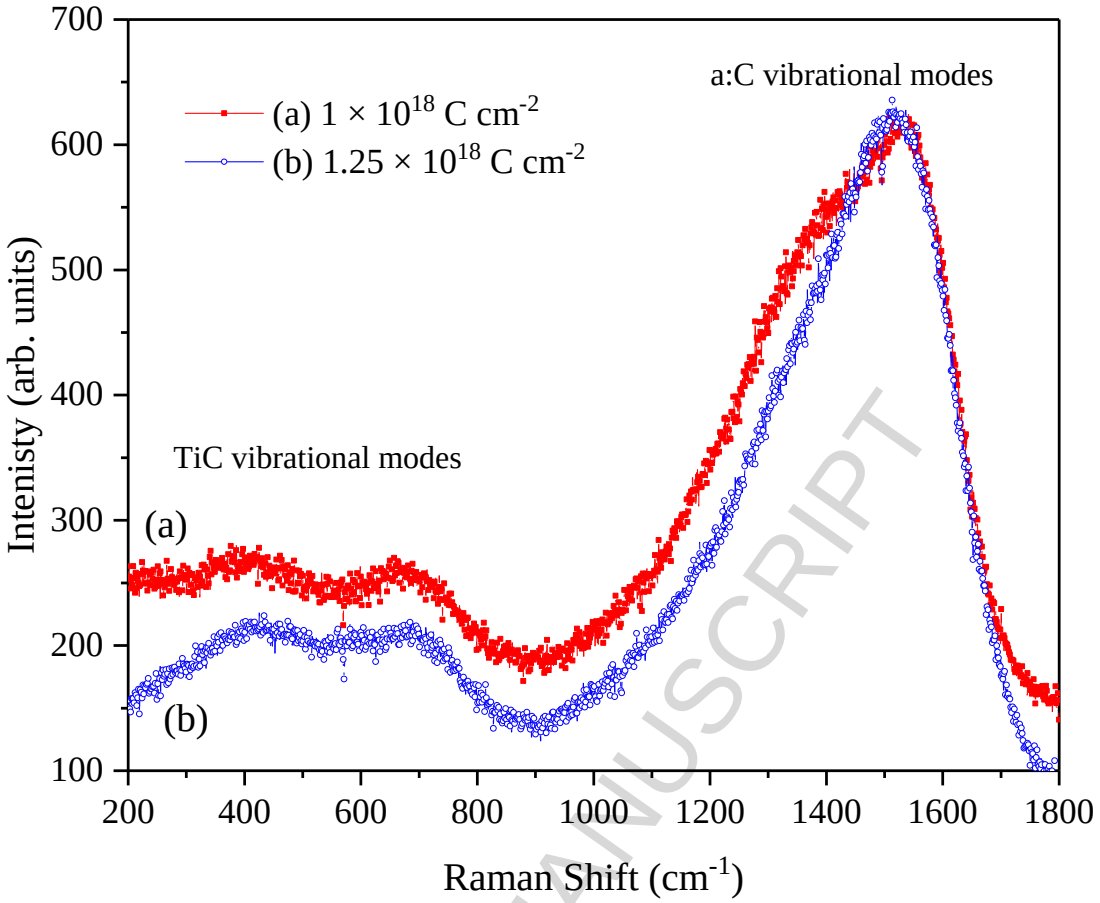

Figure 5 (color – online only)

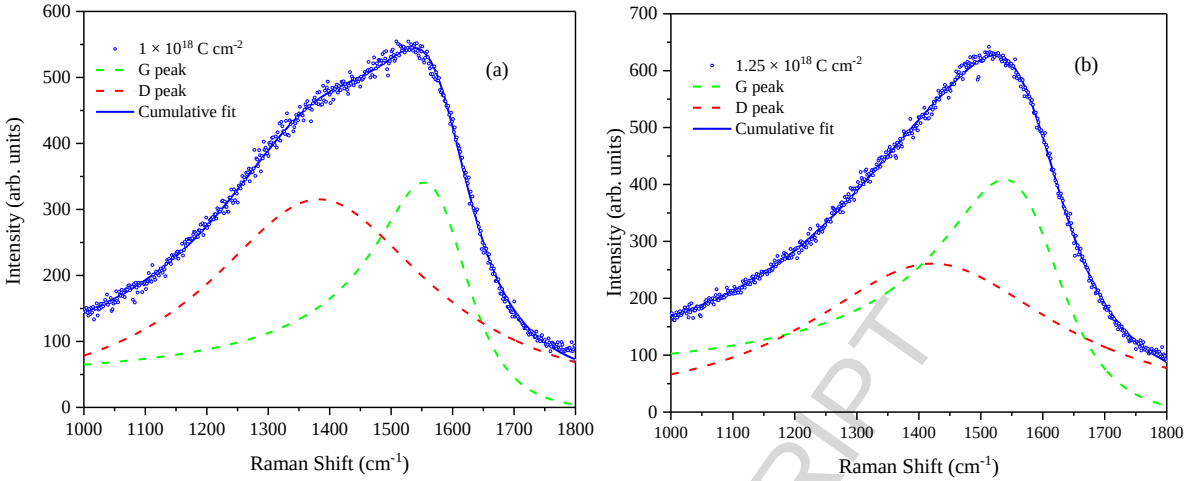

Figure 6 (color – online only)

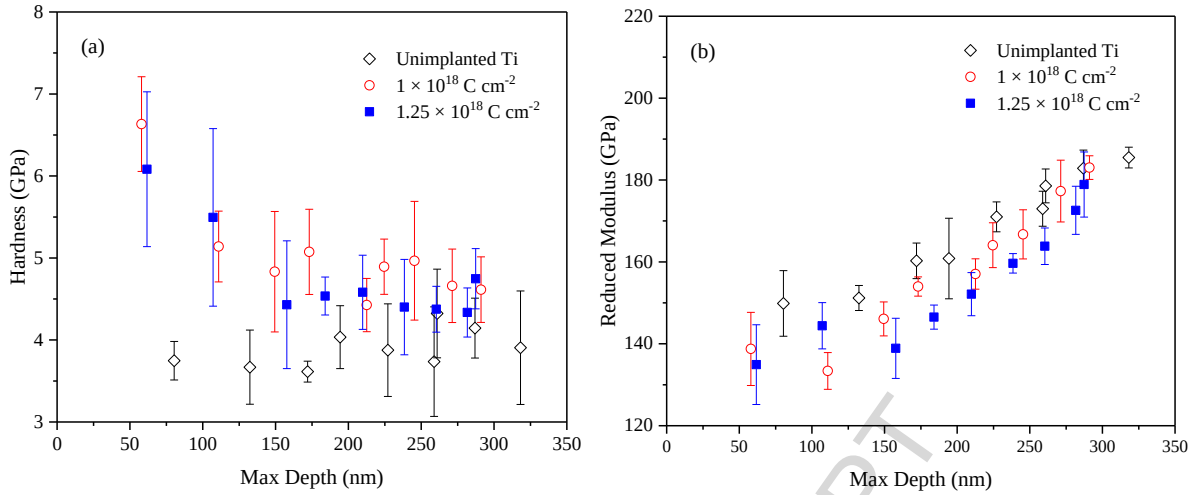

Figure 7 (color – online only)

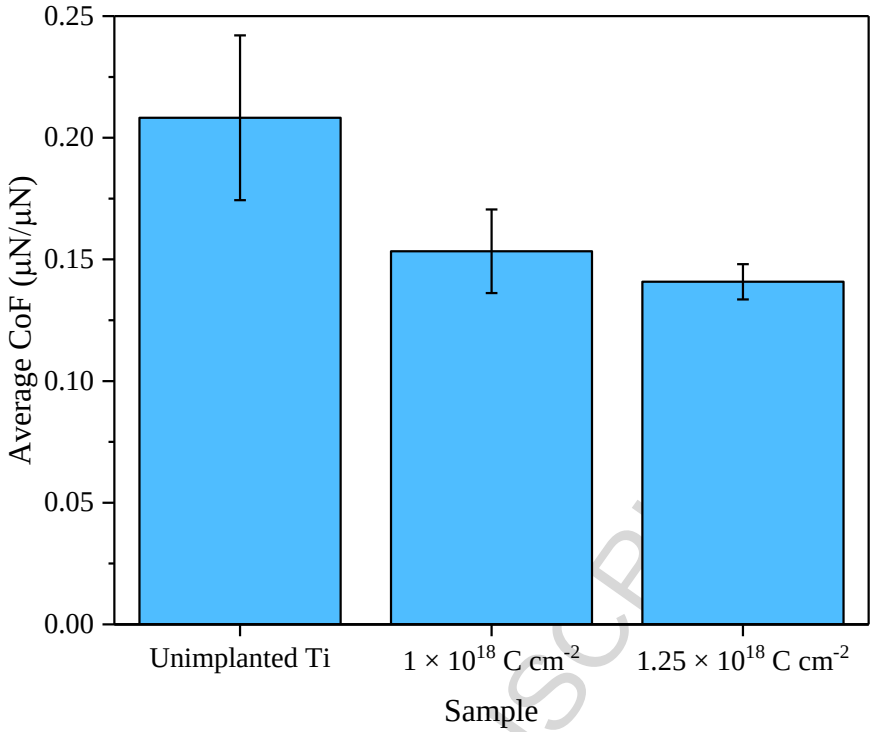

Figure 8 (color – online only)

Graphical abstract

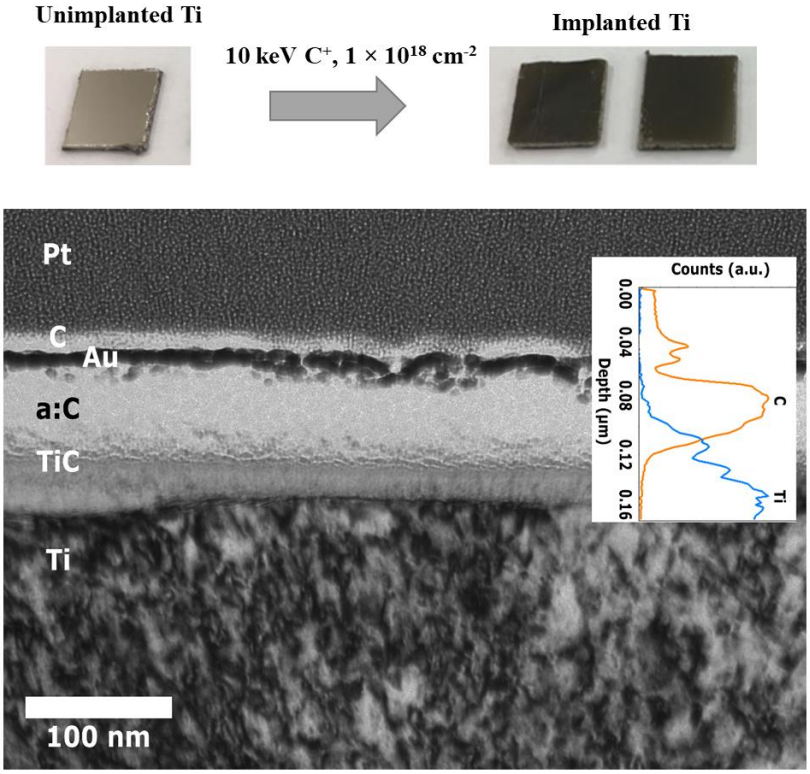

Cross-sectional TEM image of implanted Ti

Highlights

- 10 keV C implantation onto Ti at high fluence leads to decorative black surfaces
- The top surface is made of amorphous carbon (a:C) layers with 15-20% sp^3 content
- C implantation leads to an intermixing TiC layer separating a:C from Ti substrate
- This bi-layered coating leads to a black surface at a thickness as low as 100 nm
- The coating improved surface hardness by 72% and reduced friction coefficient by 25%